

## Article

# Insights into the Adsorption of Cr(VI) on Activated Carbon Prepared from Walnut Shells: Combining Response Surface Methodology with Computational Calculation

Hicham Yazid<sup>1</sup>, Taoufiq Bouzid<sup>1</sup>, El mountassir El mouchtari<sup>1,2</sup>, Lahoucine Bahsis<sup>1,\*</sup>, Mamoune El Himri<sup>1</sup>, Salah Rafqah<sup>1</sup> and Mohammadine El haddad<sup>1,\*</sup>

<sup>1</sup> Laboratory of Analytical and Molecular Chemistry (LCAM), Department Chimie—Faculty Poly Disciplinary of Safi (FPS), BP 4162, Safi 46000, Morocco; ydhicham78@gmail.com (H.Y.); taoufiq.bouzid@gmail.com (T.B.); elmountassirelmouchtari@gmail.com or el-mountassir.el-mouchtari@etu.univ-amu.fr (E.m.E.m.); m.elhimri@uca.ac.ma (M.E.H.); rafqah@gmail.com (S.R.)

<sup>2</sup> Département de Chimie et Environnement, FST Béni Mellal, Université Sultan Moulay Slimane, BP 523, Beni Mellal 23000, Morocco

\* Correspondence: bahsis.lahoucine@gmail.com or bahsis.l@ucd.ac.ma (L.B.); elhaddad71@gmail.com (M.E.h.)

**Abstract:** Walnut shells were used to produce highly microporous activated carbon. The prepared activated walnut shells were found to be an efficient adsorbent for removing Cr(VI). The study used the response surface methodology to investigate four independent variables effect: Cr(VI) concentration, pH, AC-Ws dose, and temperature on the Cr(VI) removal efficiency, which was studied in the concentration range of 0.1 to 0.3 g/L, 4 to 10, 15 to 35 °C and 1 to 5 mg/L, respectively. Through experiments designed, the optimum conditions were determined to be 4, 0.23 g/L, 298 k, and 2 g/L, respectively. At these conditions, the efficiency of removal was found to be 93%. The thermodynamic study of the adsorption process showed a spontaneous and exothermic nature. The kinetic model that explains the experimental data is the pseudo-second-order model. Furthermore, the Langmuir isotherm model was estimated to be an excellent representation of the equilibrium data. Quantum calculations and NCI analyses were also performed to get more light on the adsorption mechanism of the Cr(VI) atom and its complex form on the prepared AC-Ws surface.

**Keywords:** adsorption; Chromium (VI); walnut shell; activated carbon; experimental design



**Citation:** Yazid, H.; Bouzid, T.; El mouchtari, E.m.; Bahsis, L.; El Himri, M.; Rafqah, S.; El haddad, M. Insights into the Adsorption of Cr(VI) on Activated Carbon Prepared from Walnut Shells: Combining Response Surface Methodology with Computational Calculation. *Clean Technol.* **2024**, *6*, 199–220. <https://doi.org/10.3390/cleantechnol6010012>

Academic Editors: Miklas Scholz and Patricia Luis

Received: 19 November 2023

Revised: 23 January 2024

Accepted: 21 February 2024

Published: 26 February 2024



**Copyright:** © 2024 by the authors. Licensee MDPI, Basel, Switzerland. This article is an open access article distributed under the terms and conditions of the Creative Commons Attribution (CC BY) license (<https://creativecommons.org/licenses/by/4.0/>).

## 1. Introduction

Heavy metals occur naturally present in the earth's crust in small amounts, but they become concentrated as a result of industrial activities. Population growth and industrialization have led to environmental pollution from various pollutants, including heavy toxic metals such as copper, lead, arsenic, nickel and mercury, produced by industrial activities. Chromium, recognized for its elevated toxicity and tendency to bio-accumulate within the food chain [1] is acknowledged as one of the crucial heavy metals essential for various biological processes.

Chromium is naturally present in water sources in both hexavalent and trivalent forms. Trivalent chromium Cr(III) serves as a trace element in living organisms, hexavalent chromium is very toxic, mutagenic, and even carcinogenic even at low concentrations, making it a hazard for humans and other organisms [2]. Adverse reactions performed in the presence of Cr(VI) were reported such as lung cancer, damage to the central nervous system, gastrointestinal and cancer anemia [3]. Hexavalent chromium is discharged in large amounts each year by industries such as steel, textile, electroplating, and chrome plating, which release wastewater containing this substance [4]. The maximum concentration of Cr(VI) allowed by the EPA agency (US Environmental Protection Agency) standards is 0.05 mg/L for drinking water sources, and it's 0.1 mg/L for surface wastewater intended for

discharge into the water source. several methods such as adsorption, chemical precipitation and membrane filtration [5–8] have been considered to achieve EPA standards. In recent years, a variety of cheap adsorbents, including activated carbon made from bagasse, medlar, plant seeds, and waste paper [9–11] have been considered for Cr(VI) removal.

Additionally, optimization techniques like Response Surface Methodology (RSM) can enhance the adsorption process. RSM is a robust experimental design method that uses mathematical and statistical techniques to analyze the correlation between independent variables and construct a model for the adsorption process. One significant advantage of employing RSM is the marked reduction in the number of experiments required to determine optimal conditions, leading to considerable time and resource savings. Various technologies, either individually or in conjunction with other methods and techniques, are used to eliminate Cr(VI). Photocatalysis [12], Electrochemical [13], Precipitation [14], Microbial treatment [15], Flotation [16] adsorption [17] and plasma destruction [18] are the most common methods. Due to complexity and economic reasons, most of the mentioned approaches are not proper for removing Cr(VI) except adsorption.

Recently, walnut shells have get great attention as an excellent adsorbent material for removing a variety of contaminants from water, including heavy metals, dyes, and organic compounds due to their unique properties as a byproduct of the walnut processing industry [19]. Walnut shells surface has various functional groups like hydroxyl, carboxyl, and phenol groups which increase its adsorptive power [20]. Walnut shells have also several advantages over other adsorbents because they are abundant, renewable and inexpensive [21,22]. Compared to other types of activated carbon, walnut shell activated carbon has several advantages [23,24]. It is a sustainable source of activated carbon because walnut shells are abundant and renewable. Moreover, they contain a high concentration of lignin, cellulose and hemicellulose, proving additional functional groups for the adsorbent surface.

The process of adsorption holds numerous advantages in environmental applications. Its exceptional ability to effectively remove contaminants such as heavy metals, organic pollutants, and dyes from both liquid and gas phases stands as its foremost benefit. Moreover, its versatility spans various industries, offering a practical solution for wastewater treatment, air purification, and soil remediation without disrupting system components. Additionally, adsorption's cost-effectiveness, renewability of adsorbents, and low energy consumption make it an economically viable and sustainable choice. Its ease of integration into existing systems, environmental compatibility, and capability to handle low pollutant concentrations further establish adsorption as an efficient, adaptable, and environmentally friendly method in environmental remediation [25].

The novelty of this study comprises several significant facets. Firstly, it involves pioneering the synthesis of an efficient adsorbent derived from walnut shells, presenting a sustainable solution for environmental remediation. Secondly, the research focuses on optimizing conditions specifically tailored for the removal of Cr(VI), demonstrating a targeted and effective approach to address heavy metal contamination. Furthermore, this study introduces advanced statistical methodology, such as response surface methodology (RSM), to comprehensively analyze and optimize multiple factors influencing Cr(VI) removal. Additionally, it provides an in-depth understanding of adsorption kinetics and thermodynamics, illuminating the intricate mechanisms involved in chromium removal processes. Moreover, the study broadens its scope by confirming the Cr(VI) adsorption mechanism through a theoretical study using quantum calculations. This theoretical approach adds depth to the understanding of the adsorption process at a molecular level, enhancing the overall comprehension of the underlying mechanisms.

## 2. Materials and Methods

### 2.1. Chemical

Potassium dichromate ( $K_2Cr_2O_7$ ; 99% purity) was purchased from Sigma-Aldrich (St. Louis, MO, USA), and 1,5-diphenyl carbazide ( $C_{13}H_{14}N_4O$ ) was provided by VWR chemicals (Radnor, PA, USA). Potassium hydroxide (KOH, 0.1 mol/L) and hydrochloric acid (HCl, 0.1 mol/L) were obtained by Fischer Scientific (Hampton, NH, USA).

## 2.2. Preparation of Activated Carbon

The prepared adsorbent AC material was obtained from walnut shells using, following the procedure [26]. After washing and drying of the obtained biosource material, a crushing step was conducted to achieve a fine texture followed by the sieving of resulted powder to isolate particles between 0.2 and 2 mm. The selected fraction was mixed with the phosphoric acid solution (50% weight/volume) under stirring for 15 min. The resulting powder was then dried for 24 h at 105 °C. Carbonization occurred in a SELECTHORN oven, with a gradual temperature increase until reaching a final temperature of 500 °C for 60 min, at a heating rate of 10 °C per minute. Post-cooling, the obtained black carbon residue underwent multiple washes with 0.1 mol/L HCl and then rinsed to neutralize the pH of the prepared carbon using distilled water. The neutralized carbon powder was then dried and ground into fine particles (AC-Ws).

## 2.3. Batch Adsorption Experiments

The adsorption experiments for synthetic Cr(VI) effluent were conducted in triplicate batches A 1000 mg/L solution of Cr(VI) was made by mixing 2.828 g of  $K_2Cr_2O_7$  (potassium dichromate) in distilled water, the solution was then diluting it. On the other hand, 0.1 mol/L NaOH (sodium hydroxide) and 0.1 mol/L HCl (hydrochloric acid) solutions were used to adjust the solution pH to the desired value. The remaining Cr(VI) concentration in the filtrate was measured using spectrophotometry (Jenway 6300, Safi, Morocco) at 540 nm after adding 1,5-diphenylcarbazide reagent, as shown in Figure 1, which causes a pink color [27,28].

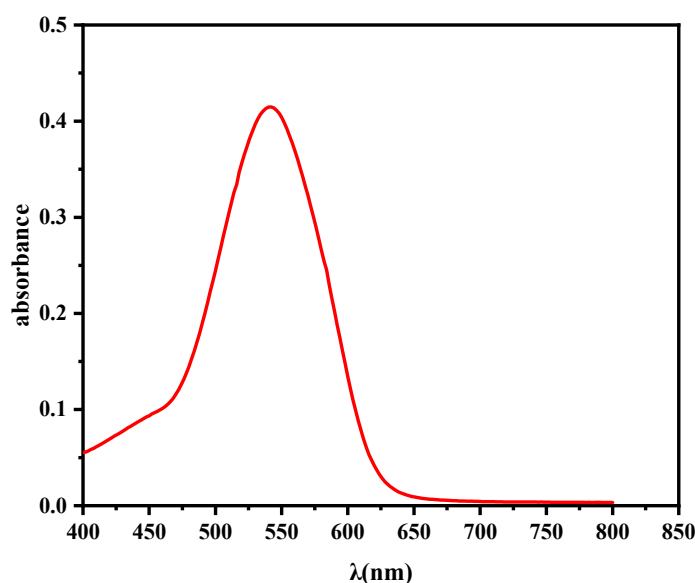


Figure 1. Specter UV-Visible of complex Cr(VI)-DPC.

Equation (1) was used to determine the percentage removal of chromium hexavalent (VI) (R%):

$$\text{Removal}(\%) = \frac{C_i - C_t}{C_i} \times 100 \quad (1)$$

The removal efficiency is R (%),  $C_i$  (mg/L) is the starting Cr(VI) concentration, and  $C_t$  mg/L is the Cr (VI) concentration at the instant t (min).

The study aimed to determine the stability of the complex formed when chromium reacts with 1,5-diphenylcarbazide (DPC) over 0–60 min (Figure 2). Results indicate that the complex between Cr(VI) and DPC is relatively stable. The complex formation time used in this research was 20 min [29].

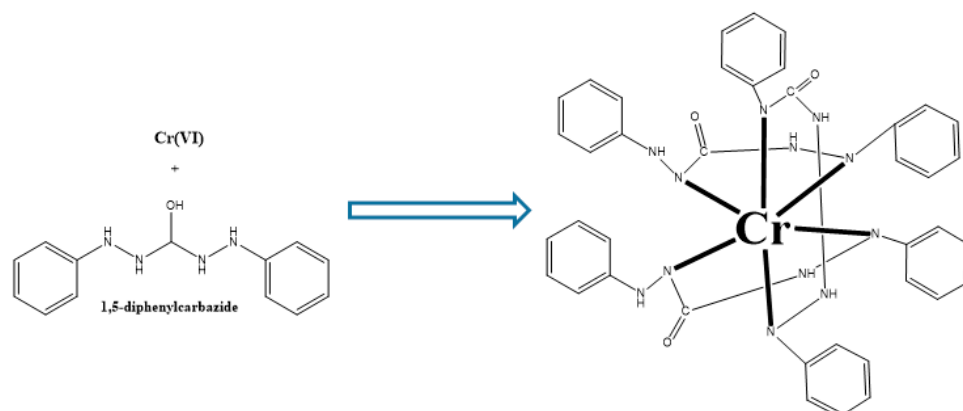


**Figure 2.** Formation of the complex Cr(VI)-DPC.

To assess the adsorption capacity of activated carbon concerning chromium (VI), adsorption experiments were conducted in a dark environment. The concentrations 1 and 5 mg/L of the Cr(VI) solutions was used in these investigations, while the material concentrations ranged between 0.1 and 0.3 g/L. Adsorption isotherms on AC-Ws were established at room temperature (25 °C) using five Cr(VI) concentrations (1, 2, 3, 4, and 5 mg/L). The mixture of AC-Ws and chromium was continuously stirred under constant magnetic agitation for 1 h to attain adsorption-desorption equilibrium.

#### 2.4. Experimental Design

The experimenters' main aim is to investigate the factors that impact a particular phenomenon and determine the optimal conditions. Specifically, their goal is to create a model that maximizes the percentage of chromium VI adsorption by adjusting various input parameters. To achieve this, they utilized the AZURAD<sup>®</sup> software to develop a design for the experiment. The experiment's design included modeling the percentage of Cr(VI) adsorption based on four variables: AC-Ws dose (Factor  $X_1$ ), pH (Factor  $X_2$ ), temperature (Factor  $X_3$ ), and concentration of chromium (VI) (Factor  $X_4$ ). Table 1 displays the experimental design and its corresponding factors.

**Table 1.** The quantitative factors of experimental design are the domain of interest.

| Factor | Name                     | Unit | Central Value | Range of Variation |
|--------|--------------------------|------|---------------|--------------------|
| $X_1$  | Dose of AC-Ws            | mg   | 10            | 5                  |
| $X_2$  | pH                       |      | 7             | 3                  |
| $X_3$  | T                        | °C   | 25            | 10                 |
| $X_4$  | Concentration of Cr (VI) | mg/L | 3             | 2                  |

#### 2.5. Computational Methods

Quantum calculations were carried out using the Forcefield code that was implemented in Gaussian 09 [30]. The optimized molecular geometry prepared activated carbon (AC) surface model was performed using universal parameterization of the force field [31]. To reveal the interaction nature between the AC surface and the chromium (VI) atom, noncovalent interaction (NCI) analyses have also been carried out using Multiwfn [32] and the VMD software was used to visualize the NCI analyses [33]. The color map can be used to show the type of interactions that occur between the adsorbent and the adsorbate. The colors red, blue, and green correspond to steric repulsions, van der Waals interactions and hydrogen bonding, respectively [34]. The adsorption energy ( $E_{ads}$ ) was calculated based on the optimized structures of the Cr(VI) complex and the AC-Ws surface using the following equation (Equation (2)):

## Adsorption of Cr(VI) complex on AC surface model

$$E_{\text{ads}} = E_{\text{Cr(VI)}} + E_{\text{AC surface}} - E_{\text{Cr(VI)-AC surface}} \quad (2)$$

### 3. Results

#### 3.1. Characterization of Activated Carbon

An essential step in identifying the kinds and numbers of functional groups present on the surface of the AC is the Boehm analysis. The assessment of basic groups on the surface, as shown by AC-Ws (mmol/L), and acidic functional groups, including carboxylic acids, phenols, and lactones, is made possible by this technique. Important information about the surface chemistry and possible adsorption mechanisms of the activated carbon can be obtained by measuring these functional groups [35,36]. In contrast to the bibliographic data on activated carbon coffee waste [37] and activated carbon capsicum annum L, the AC-Ws obtained from the activation process with a 1:1 ratio of raw material to  $\text{H}_3\text{PO}_4$  primarily consist of lactones 0.11 mmol/g, phenols 0.22 mmol/g followed by and carboxylic groups 0.75 mmol/g, as shown in Figure 3 [27].

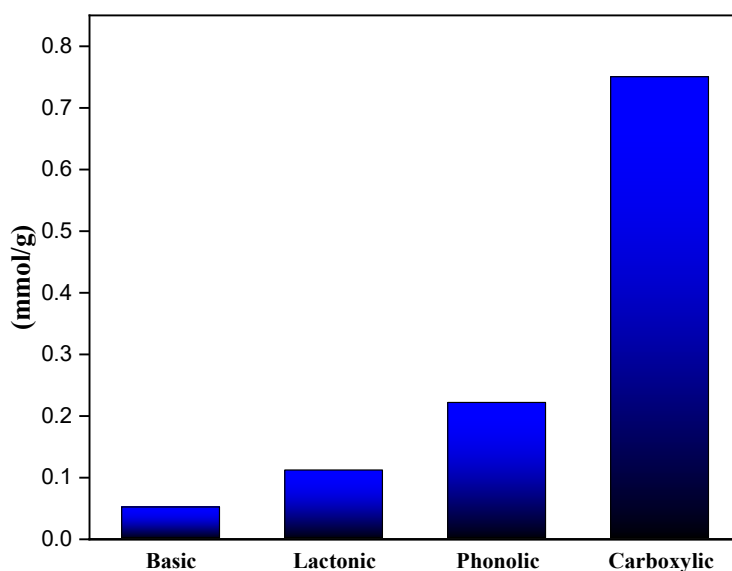


**Figure 3.** Functional groups presented on the AC-Ws surface.

Figure 4 shows only the FTIR spectrum of AC. Based on the findings, the peak observed at  $3379 \text{ cm}^{-1}$  in the spectrum is assigned to the extensional vibrations of the hydroxyl groups bound to the material. This spectroscopic feature indicates the presence and specific interaction of OH groups in the material's structure. The distinct peak located at  $1568 \text{ cm}^{-1}$  confirms the presence of C=C bonds [38]. Additionally, the band at  $1547 \text{ cm}^{-1}$  is assigned to C-O bonds deformations [39–41]. These observed absorption bands provide compelling evidence of the characteristic bonds found in walnut shell powder.

The thermogram presented in Figure 5 for the AC-Ws sample reveals distinct phases of mass reduction. Initially, between 18 and  $100 \text{ }^\circ\text{C}$ , a 21.6% mass loss is observed, attributed to the evaporation of water molecules adsorbed on the surface of the activated carbon. Subsequently, in the temperature range of 100 to  $1000 \text{ }^\circ\text{C}$ , there is a substantial 74.4% reduction in the mass of AC-Ws, primarily indicative of the combustion of the carbonaceous material. Notably, temperatures exceeding  $550 \text{ }^\circ\text{C}$  suggest the feasibility of conducting pyrolysis, thereby affirming the appropriateness of selecting  $500 \text{ }^\circ\text{C}$  as the temperature for the process of physical activation. This detailed analysis of the thermogram provides valuable insights into the thermal behavior of the AC-Ws sample, offering a better understanding of the underlying processes involved in its mass reduction across different temperature ranges.

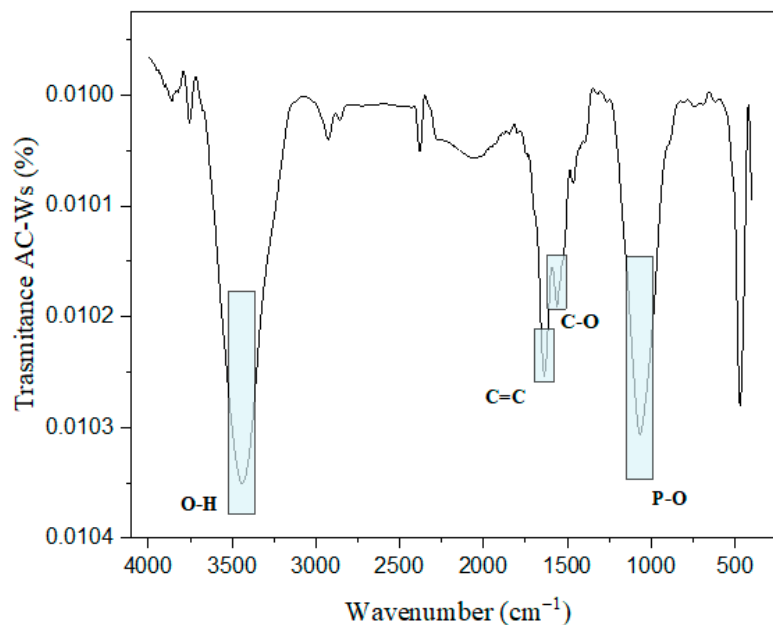


Figure 4. FTIR analysis of prepared AC-Ws.

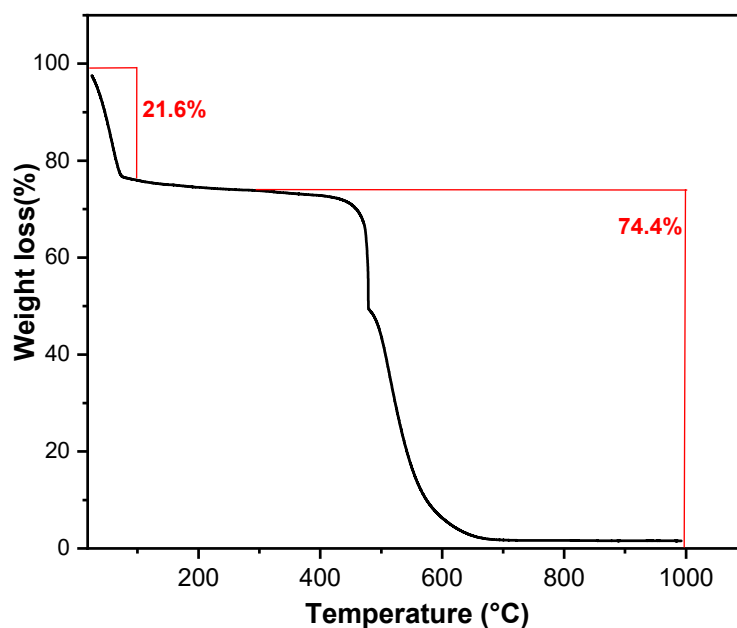
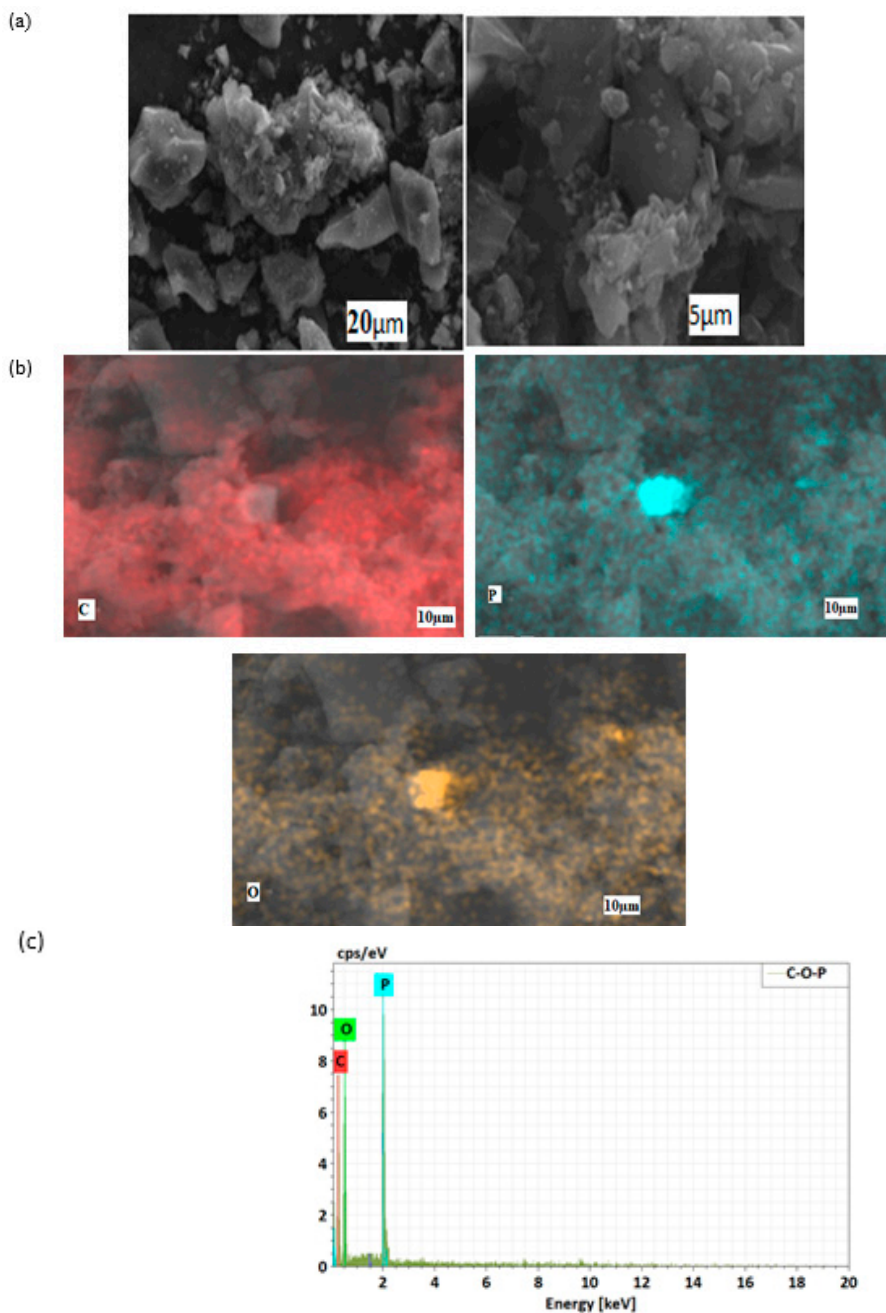


Figure 5. TGA analysis of AC-Ws.

Figure 6 depicts the surface morphology of the activated carbon. The surface in Image (a) showcases numerous pores, dark spots, and cavities, indicating that the adsorbent's surface is potentially effective for adsorbing pharmaceutical products. The element nature and their dispersion on the AC surface were analyzed using EDX analyzer and the obtained findings were summarized in Figure 6b,c. The EDX analyses confirm the presence of oxygen (O) and carbon (C) elements, revealing the existence of organic functionalities that serve as potential adsorption sites. Phosphor element observed on the AC surface was from the activation procedure through  $\text{H}_3\text{PO}_4$ .



| Element    | At. No | Netto | Mass[%] | Mass Norm.[%] | Atom [%] | Abs.error [%] (1 sigma) | Rel.error[%] (1 sigma) |
|------------|--------|-------|---------|---------------|----------|-------------------------|------------------------|
| Carbon     | 6      | 1271  | 69.7    | 43.35         | 53.23    | 14.82                   | 21.25                  |
| Oxygen     | 8      | 1701  | 70.65   | 43.94         | 40.5     | 13.94                   | 19.73                  |
| Phosphorus | 15     | 2807  | 15.45   | 9.61          | 4.58     | 0.74                    | 4.78                   |
|            |        | Sum   | 160.79  | 100.00        | 100.00   |                         |                        |

Figure 6. The AC-Ws analyses using (a) SEM, (b) elemental cartography and (c) EDX analysis.

The zero point charge ( $pH_{pzc}$ ) of powdered carbon is a crucial property in adsorption processes, particularly in the presence of electrostatic forces [42]. It corresponds to the pH at which the surface of activated carbon powder is neutrally charged. The  $pH_{pzc}$  value for the AC-Ws adsorbent is 4.1. The surface charge is positive for solutions with a pH below 4.1 and becomes negative for solutions with a pH above this value (see Figure 7).

Remarkably, pH environments significantly vary for chromium species:  $H_2CrO_4$  mainly exists at pH levels below 2, while  $HCrO_4^-$  and  $Cr_2O_7^{2-}$  are primarily present in the pH range of 2 to 6.8. Furthermore,  $CrO_4^{2-}$  is predominant in pH environments greater than 6.8 [43,44]. Consequently, both anions,  $HCrO_4^-$  and  $Cr_2O_7^{2-}$ , are more adsorbed onto the activated carbon surface at a pH below the zero point charge ( $pH_{pzc}$ ).

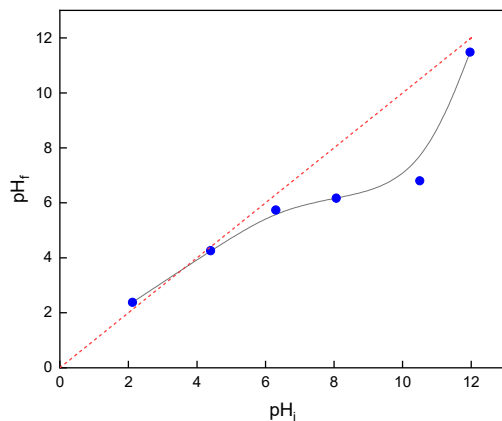


**Figure 7.** Variation of  $pH_f$  as a function  $pH_i$  to determine the  $pH_{pzc}$  of the AC-Ws.

### 3.2. Experimental Design

The model enables the representation of the percentage of adsorption for different input parameter variations. A 2nd-degree polynomial model has been selected, as shown in the general equation (Equation (3))

$$Y = b_0 + \sum_{i=1}^n b_i X_i + \sum_{i=1}^n b_{ii} X_i^2 + \sum_{i=1}^n \sum_{j=i+1}^n b_{ij} X_i X_j \tag{3}$$

where  $Y$  is the response variable that we are trying to predict or model,  $b_i$  is the linear coefficient,  $b_0$  is the constant,  $b_{ij}$  is the cross-product coefficient,  $b_{ii}$  is the squared coefficient,  $X_j$  and  $X_i$  are the independent variables.

In our case is written as follows (Equation (4))

$$Y = b_0 + b_1 X_1 + b_2 X_2 + b_3 X_3 + b_4 X_4 + b_{11} X_1^2 + b_{22} X_2^2 + b_{33} X_3^2 + b_{44} X_4^2 + b_{12} X_1 X_2 + b_{13} X_1 X_3 + b_{14} X_1 X_4 + b_{23} X_2 X_3 + b_{24} X_2 X_4 + b_{34} X_3 X_4 \tag{4}$$

To improve the accuracy of coefficient estimation in the polynomial model and make it more applicable for predictive purposes [45,46], we conducted a comprehensive experimental design consisting of 27 experiments using a composite matrix. It is worth noting that Experiment 17 was replicated three times to assess and quantify experimental variability. Table 2 presents the experimental conditions and corresponding percentages of Cr(VI) adsorption achieved after one hour of equilibrium time.

**Table 2.** Shows the experimental design conditions and the amount of Cr (VI) adsorption (Y).

| Experiment | Mass of AC-Ws (mg) | pH | T (°C) | Concentration of Cr(VI) (mg/L) | Y (%) |
|------------|--------------------|----|--------|--------------------------------|-------|
| 1          | 5                  | 4  | 15     | 1                              | 95.0  |
| 2          | 15                 | 4  | 15     | 1                              | 100   |
| 3          | 5                  | 10 | 15     | 1                              | 55.6  |
| 4          | 15                 | 10 | 15     | 1                              | 55.6  |
| 5          | 5                  | 4  | 35     | 1                              | 88.65 |
| 6          | 15                 | 4  | 35     | 1                              | 97.0  |
| 7          | 5                  | 10 | 35     | 1                              | 41.5  |
| 8          | 15                 | 10 | 35     | 1                              | 45.6  |

Table 2. Cont.

| Experiment | Mass of AC-Ws (mg) | pH | T (°C) | Concentration of Cr(VI) (mg/L) | Y (%) |
|------------|--------------------|----|--------|--------------------------------|-------|
| 9          | 5                  | 4  | 15     | 5                              | 70.26 |
| 10         | 15                 | 4  | 15     | 5                              | 85.56 |
| 11         | 5                  | 10 | 15     | 5                              | 30.56 |
| 12         | 15                 | 10 | 15     | 5                              | 35.65 |
| 13         | 5                  | 4  | 35     | 5                              | 63.0  |
| 14         | 15                 | 4  | 35     | 5                              | 80.23 |
| 15         | 5                  | 10 | 35     | 5                              | 35.23 |
| 16         | 15                 | 10 | 35     | 5                              | 48.6  |
| 17         | 5                  | 7  | 25     | 3                              | 55.5  |
| 18         | 5                  | 7  | 25     | 3                              | 54.9  |
| 19         | 5                  | 7  | 25     | 3                              | 55.3  |
| 20         | 15                 | 7  | 25     | 3                              | 60.3  |
| 21         | 10                 | 4  | 25     | 3                              | 90.0  |
| 22         | 10                 | 10 | 25     | 3                              | 38.0  |
| 23         | 10                 | 7  | 15     | 3                              | 50.0  |
| 24         | 10                 | 7  | 35     | 3                              | 45.6  |
| 25         | 10                 | 7  | 25     | 1                              | 60.0  |
| 26         | 10                 | 7  | 25     | 5                              | 40.6  |
| 27         | 10                 | 7  | 25     | 3                              | 50.6  |

### 3.3. Validation of Model

After conducting 27 experiments to design and measure the quantities of adsorbed hexavalent chromium Cr(VI), the model parameters were estimated by multilinear regression. The resulting Equation (4) illustrates this estimation model.

$$Y = 51.86 + 3.99 X_1 - 21.29 X_2 - 1.82 X_3 - 8.29 X_4 + 6.53 X_1^2 + 11.92 X_2^2 - 4.27 X_3^2 - 1.77 X_4^2 - 1.45 X_1 X_2 + 1.10 X_1 X_3 + 2.09 X_1 X_4 + 0.96 X_2 X_3 + 2.08 X_2 X_4 + 2.40 X_3 X_4 \quad (5)$$

The variance of the experiment was calculated from the triplicate (Experiment 17, 18, and 19) and showed excellent repeatability of the measurements. Thus, the variability observed in the outcomes is solely determined by the variability of the factors included in the matrix, rather than by the experimenter [47].

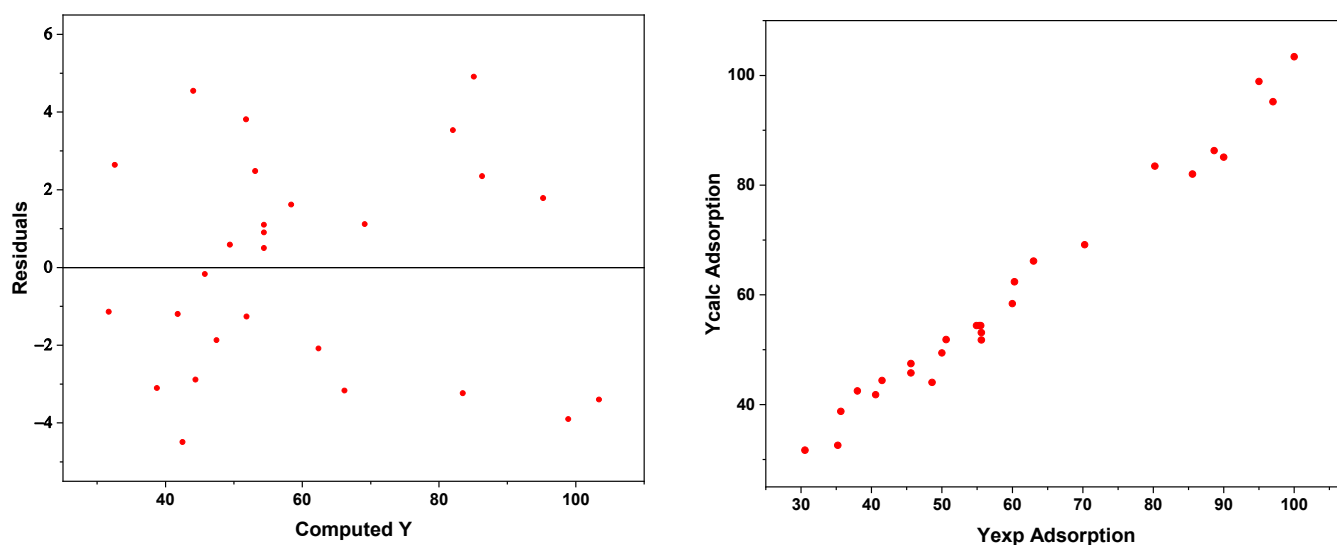
Table 3 displays the ANOVA results, which indicate that the model's quadratic, linear, and interaction terms are statistically significant. Table 3 demonstrates that the estimated model has a high degree of effectiveness and significance, as indicated by the *p*-value and  $R^2$ . Specifically, the probability value for the model is less than  $10^{-4}$ , which suggests that the model accurately describes the variation of results for both responses. Additionally, the small difference of 0.02 between the predicted and the fitted coefficient confirms that the model has good predictive capacity, as this value is below the threshold of 0.2.

Table 3. ANOVA analysis for the Cr(VI) adsorption percentage and degradation.

|             | Squares Sum | Freedom Degrees | Mean Square | Ratio   | <i>p</i> -Value % | $R^2$ | $R^2_{Adj}$ |
|-------------|-------------|-----------------|-------------|---------|-------------------|-------|-------------|
| Regression  | 11.007      | 14              | 786.220     | 8423.78 | 0.000 ***         | 0.98  | 0.96        |
| Residuals   | 197.687     | 12              | 16.474      |         |                   |       |             |
| Lack of fit | 197.501     | 10              | 19.750      | 211.608 | 0.471 **          |       |             |
| Error       | 0.187       | 2               | 0.093       |         |                   |       |             |
| Total       | 11.204      | 26              |             |         |                   |       |             |

Figure 8 illustrates the variability in residuals, representing the difference between the model-based calculated values ( $Y_i$  cal) and the corresponding experimental values ( $Y_i$  exp), plotted against the response calculated by the model. The residuals exhibit a random distribution on both sides of the axis, predominantly clustering around zero. This

pattern suggests that the majority of residuals closely approach zero, validating the model's accuracy in representing the experimental data.



**Figure 8.** Residual graphs show the percentage of adsorption  $Y_{ical}$  as a function of  $Y_{ilexp}$ .

### 3.4. 3D Surfaces, Contour and Perturbation Plots

The AZURAD software was used to generate iso-response curves that show the variable's effect on the removal of Cr(VI). Figure 9a,b illustrates that the adsorption rate decreases as pH increases, regardless of the temperature. For instance, at pH = 4, the adsorption rate is 85%, while at pH = 9, it drops to 42.56%. This is because  $HCrO_4$  is the most common chromium form at low pH values. This causes protonation of the AC-Ws surface with  $H^+$  ions, leading to the Colombian attraction between the negatively charged chromium ions and the positively charged AC-Ws surface. At higher pH levels, the more prevalent forms of chromium are  $CrO_4^{2-}$  and  $Cr_2O_7^{2-}$ , this means that the surface of the AC-Ws is less likely to be protonated by  $OH^-$  ions, resulting in electrostatic repulsion between the chromium ions and the negatively charged surface of the AC-Ws [48]. The study illustrated in Figure 9c,d reveals that as the amount of AC-Ws increases, there's a slight uptick in removal efficiency. This is assigned to the binding zones presented on the surface of AC-Ws for complexation, as stated in reference [49]. However, as the Cr(VI) concentration increases from 1 to 5 mg/L at pH = 4, the data in Figure 9e,f demonstrates a decline in removal efficiency from 91.07% to 78.95%. This decrease is caused by a low ratio of adsorbent surface-active sites to total metal ions in the solution at increasing metal ion concentrations, resulting in a limited number of metal ions that can interact and be eliminated from the solution.

### 3.5. Optimization and Validation of Result

To identify the optimized reaction conditions, adjustments were made to the AC-Ws dosage, pH and concentration of Cr(VI) in the AZURAD@ software (<http://www.azurad.fr/>, accessed on 18 November 2023). This was done to obtain the maximum desirability function, and the outcomes are presented in Figure 10. According to the study, a concentration of 2 mg/L, a pH of 4, an AC-Ws dosage of 0.23 g/L, and a removal effectiveness of 93% were the most favorable parameters for eliminating Cr(VI). These facts match with previously published research, specifically for the water pH, as seen in Table 2. The desirability function of 1.0 indicates that the conditions are favorable for removing Cr(VI) using AC-Ws.

The study aimed to determine the optimal parameters for Cr(VI) removal using the AC-Ws adsorbent, and the results showed that the response surface methodology was effective for this purpose. The study utilized numerical optimization to set the pH, AC-Ws dosage, and Cr(VI) concentration, to achieve the highest removal efficiency. The optimal conditions

were found to be a pH of 4, an AC-Ws dosage of 0.23 g/L, and a Cr(VI) concentration of 2 mg/L, which resulted in a removal efficiency of 93%. These results meet with previous investigations(as shown in Table 2). The desirability function of 1.0 indicated that the conditions were suitable for removing Cr(VI) using AC-Ws. Figure 10 presents the optimal values for each variable and the desirability function.

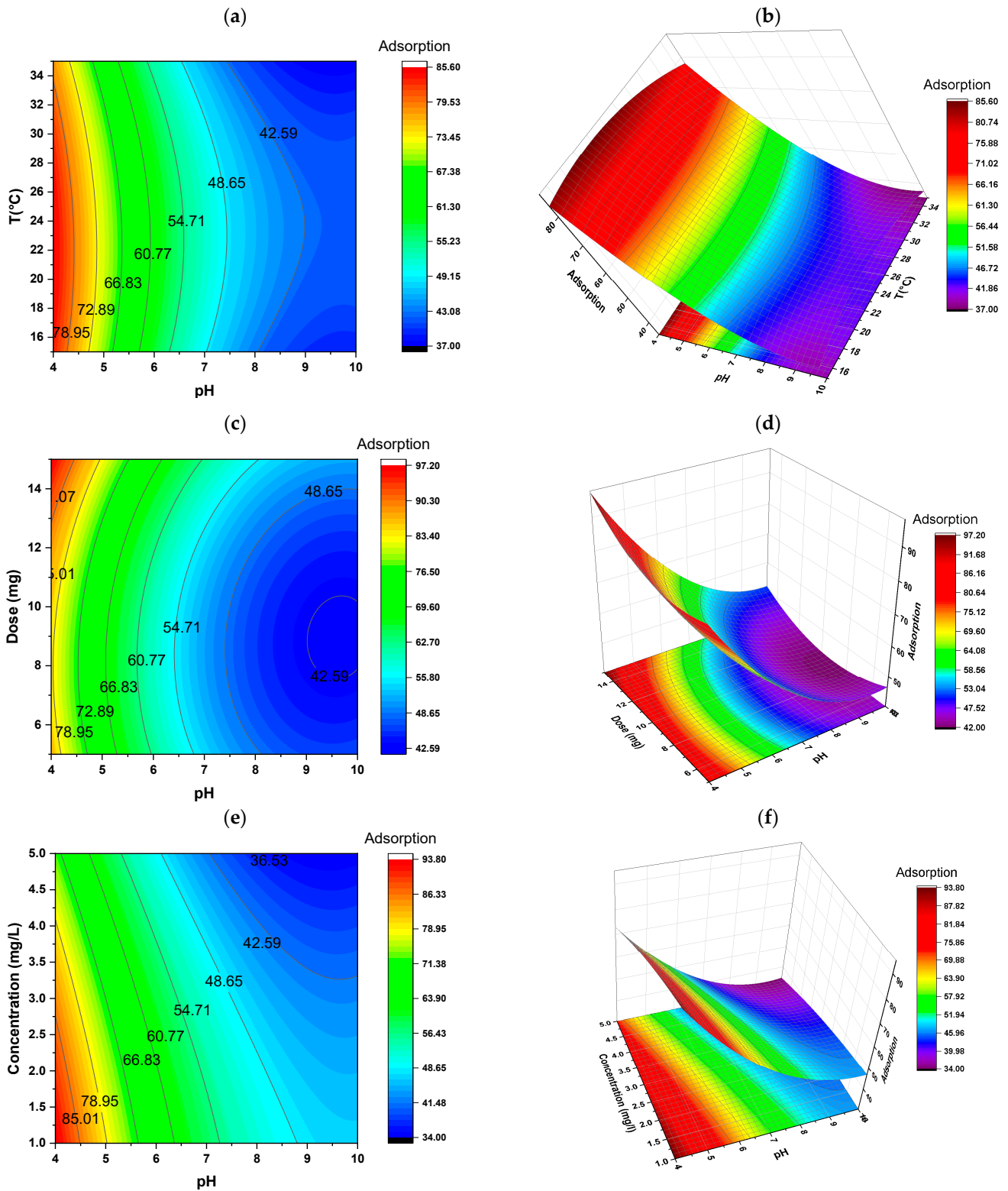
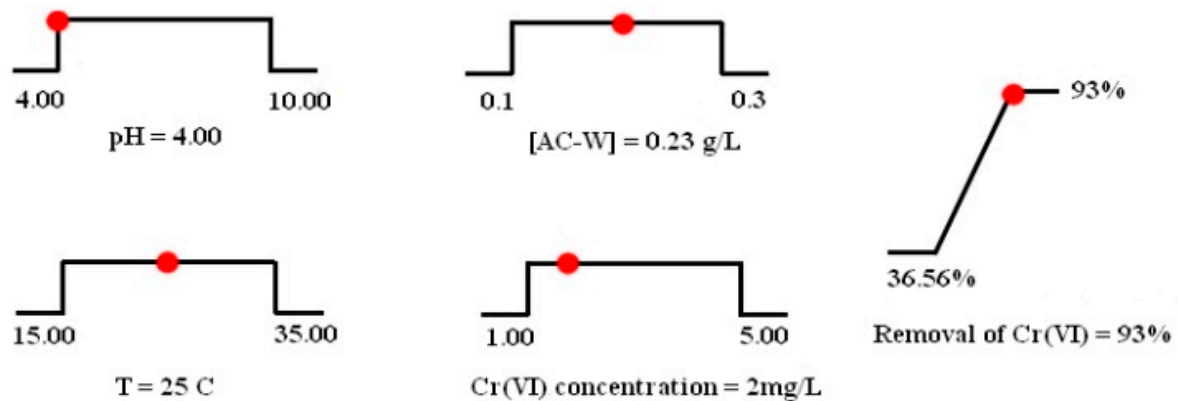


Figure 9. Response surface plot the adsorption of Cr(VI) changes with variations in temperature, pH, concentration of Cr(VI), and dose AC-Ws.



**Desirability = 1.00**

**Figure 10.** The optimal value of the parameters and desirability function.

### 3.6. Kinetics Study

Adsorption kinetics were utilized to investigate the adsorption mechanism of various models, including diffusion control, chemical reaction, and mass transfer coefficient. These models are represented by PFO (pseudo-first-order) (Equation (6)) and PSO (pseudo-second-order) (Equation (7)). The linearized form of these models is provided below [44,45]:

$$\log(q_e - q_t) = \log(q_e) - \frac{K_1 t}{2.303} \quad (6)$$

$$\frac{t}{q_t} = \frac{1}{K_2 q_e^2} + \frac{t}{q_e} \quad (7)$$

With  $q_e$  (equilibrium adsorption capacity);  $q_t$  (adsorption capacity) and time ( $t$ ), respectively,  $K_1$  ( $\text{min}^{-1}$ ) and  $K_2$  ( $\text{g}/\text{mg}\cdot\text{min}$ ) are the PFO and PSO rate constant is, respectively, calculated in [50–52].

The models used in this study were evaluated based on the parameters illustrated in Table 4 and Figure 11. The kinetic data obtained from the experiment were analyzed using the determination coefficient  $R^2$  and equilibrium adsorption capacity. The outcomes demonstrated that compared to the FSO model, the PSO model suited the experimental data better and had a higher  $R^2$  value. Furthermore, it was discovered that the estimated  $q_e$  values for the PSO model and the observed  $q_e$  values agreed rather well, indicating a superior fit compared to the PFO model. Based on these findings, the PSO model was considered appropriate for explaining the adsorption mechanism and it was determined that the chemisorption mechanism governed the adsorption process, as previously reported [53].

**Table 4.** Kinetic models parameters for Cr(VI) adsorption by AC-Ws.

| Concentration of Cr(VI) (mg/L) | Pseudo First-Order        |                           |                             |       | Pseudo Second-Order       |                                 |       |
|--------------------------------|---------------------------|---------------------------|-----------------------------|-------|---------------------------|---------------------------------|-------|
|                                | $Q_{e,\text{exp}}$ (mg/g) | $Q_{e,\text{cal}}$ (mg/g) | $K_1$ ( $\text{min}^{-1}$ ) | $R^2$ | $Q_{e,\text{cal}}$ (mg/g) | $k_2 \times 10^{-2}$ (g/mg·min) | $R^2$ |
| 1                              | 3.212                     | 2.6                       | 0.0599                      | 0.952 | 20.94                     | 3.584                           | 0.995 |
| 2                              | 6.645                     | 6.223                     | 0.0598                      | 0.894 | 44.2                      | 7.692                           | 0.992 |
| 3                              | 9.748                     | 7.261                     | 0.0391                      | 0.961 | 22.66                     | 10.75                           | 0.991 |
| 4                              | 12.944                    | 10.185                    | 0.0414                      | 0.937 | 12.11                     | 14.705                          | 0.993 |
| 5                              | 14.905                    | 11.634                    | 0.0598                      | 0.959 | 16.814                    | 19.607                          | 0.995 |

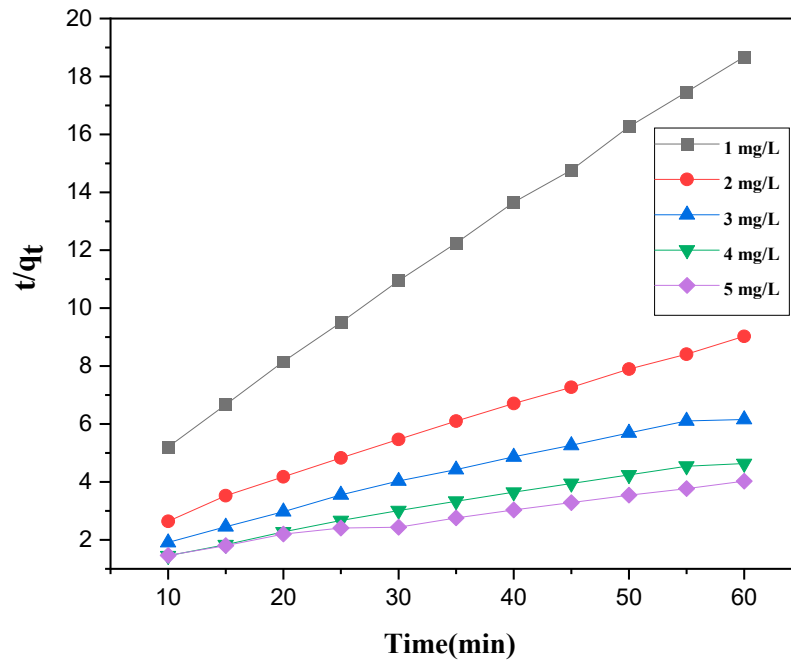


Figure 11. PSO kinetic modelling was applied to Cr(VI) adsorption on AC-Ws.

3.7. Equilibrium Study

Freundlich and Langmuir isotherms were used to analyze the equilibrium. Equations (8) and (9) reflect the linearized versions of these models [54]:

$$\frac{C_e}{q_e} = \frac{1}{q_m K_L} + \frac{1}{q_m} C_e \tag{8}$$

$$\log(q_e) = \log(K_f) + \frac{1}{n} \log(C_e) \tag{9}$$

The parameters for the Langmuir isotherm model include the equilibrium capacity  $q_e$ , the concentration  $C_e$ , the Langmuir constant  $q_m$ , for the maximum monolayer adsorption capacity, and the Langmuir constant  $K_L$  associated with the free energy of adsorption. Adsorption intensity and capacity are additionally affected by the constants  $K_f$  and  $n$ . Table 5 presents the experimental isotherm parameters, which were determined at constant pH = 4 with starting Cr(VI) concentrations ranging from 1 to 5 mg/L at four different temperatures.

Table 5. Hexavalent chromium isotherm constants at various temperatures.

| Temperature | Langmuir Model |       |       | Freundlich Model |       |       |
|-------------|----------------|-------|-------|------------------|-------|-------|
|             | $Q_m$ (mg/g)   | $R_L$ | $R^2$ | $K_F$            | $1/n$ | $R^2$ |
| 293K        | 38.46          | 0.641 | 0.99  | 22.13            | 0.42  | 0.96  |
| 303K        | 41.56          | 0.472 | 0.98  | 32.25            | 0.312 | 0.95  |
| 313K        | 48.23          | 0.373 | 0.99  | 41.65            | 0.224 | 0.97  |
| 323K        | 52.42          | 0.308 | 0.99  | 57.81            | 0.202 | 0.94  |

The Langmuir and Freundlich models offer precise depictions of Cr(VI) adsorption on AC. The coefficient of determination ( $R^2$ ) was used to determine the most appropriate model for representing the experimental data. Figure 12 and Table 5 show that the Langmuir model is the most appropriate. It has a coefficient of determination greater than or equal to 0.99, and the  $R_L$  (separation factor) values fall within the range of 0 to 1, indicating favorable adsorption conditions. According to the Langmuir model, the adsorption of Cr(VI) occurs as a monolayer, implying a uniform surface area of the adsorbent and negligible interactions

between adsorbed molecules. Furthermore, the theoretical Langmuir adsorption capacity of the composites closely matches the experimental results.

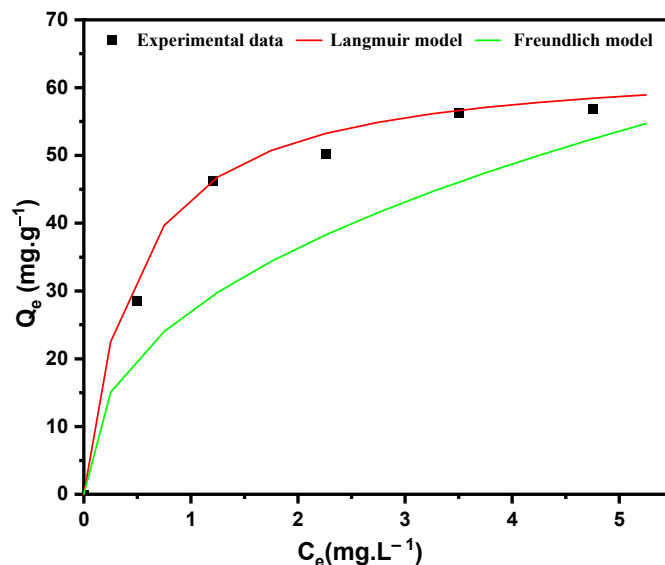


Figure 12. Experimental data and non-linear isotherms obtained for Cr(VI) adsorption with AC-Ws.

Table 6 compares the AC-Ws adsorption capacity for Cr(VI) to that of other adsorbents. The data shows that AC-Ws have a higher adsorption capacity than other adsorbents. The difference in adsorption capacity is assigned to the specific characteristics of the adsorbents, such as surface area, functional groups, and structure.

Table 6. AC-Ws adsorption capacity along with other adsorbents.

| Adsorbent              | Q <sub>max</sub> (mg·g <sup>-1</sup> ) | pH | Reference  |
|------------------------|--|----|------------|
| Walnut Shell AC-Ws     | 59.76                                  | 4  | This study |
| Palm Kernel Shell      | 8.2                                    | 4  | [55]       |
| ACSBB                  | 52.5                                   | 4  | [56]       |
| Palm shell AC          | 12.6                                   | 4  | [57]       |
| Coconut Shell charcoal | 10.8                                   | 4  | [58]       |
| Almond Shell           | 2.4                                    | 4  | [59]       |

### 3.8. Adsorption Process Thermodynamics

To study the thermodynamic properties of the process, the thermodynamic adsorption was conducted at optimal conditions at various temperatures (from 20 to 50 °C with an interval of 10 °C). we determined the thermodynamic constants such as entropy change (ΔS°), enthalpy change (ΔH°), and Gibbs free energy change (ΔG°) using the following equations (Equations (10)–(12)) [60].

$$K = \frac{q_e}{C_e} \tag{10}$$

$$\Delta G^\circ = -RT \ln K \tag{11}$$

$$\ln K = \frac{\Delta S^\circ}{R} - \frac{\Delta H^\circ}{RT} \tag{12}$$

where K (L/g) is the equilibrium constant, the adsorption capacity is q<sub>e</sub> (mg/g) the equilibrium concentration of Cr(VI) is C<sub>e</sub> (mg/L) R is the universal gas constant and the temperature is T (K).

The thermodynamic properties of the adsorption process are listed, along with their numerical values. A negative ΔH° highlight the exothermicity of the process, a positive ΔS° suggests an increase in randomness at the solid/solution interface, and a negative ΔG°

means that the process is spontaneous and becomes more favorable at higher temperatures as the negative  $\Delta G^\circ$  value increases with temperature (Table 7).

**Table 7.** Cr(VI) adsorption thermodynamic characteristics on AC-Ws.

| T (K) | $\Delta G$ (kJ·mol <sup>-1</sup> ) | $\Delta S$ (J·mol <sup>-1</sup> ·K <sup>-1</sup> ) | $\Delta H$ (kJ·mol <sup>-1</sup> ) |
|-------|------------------------------------|--|------------------------------------|
| 293   | -36.20                             |  |                                    |
| 303   | -41.99                             |  |                                    |
| 313   | -43.77                             | 212.45   | -28.596676                         |
| 323   | -45.56                             |  |                                    |

### 3.9. Mechanism of Adsorption of Cr(VI) on AC-Ws Surface

The way that Cr(VI) sticks to activated carbon (AC-Ws) is affected by many things, like the stuff the AC-Ws are made of, the shape of the Cr(VI) molecules, and the way they come together. The FT-IR test of AC-Ws has bumps at 3444.1 cm<sup>-1</sup>, which means that the O-H bits are being pulled and stretched. [61]. These groups were detected by FT-IR peaks at 1071.43 cm<sup>-1</sup>, 1467.83 cm<sup>-1</sup>, 1641.62 cm<sup>-1</sup>, 2871.04 cm<sup>-1</sup> and 2915.56 cm<sup>-1</sup>. Additionally, the surface contains specific functional groups, including C-H, -OH, -COOH, and -CH<sub>3</sub>, as confirmed by Boehm titration, which identified several adsorption sites such as C=C, P-O-C, P=O bonds, and acid phosphate ester bonds. To grasp how hydrogen bonding works and which functional groups act as hydrogen donors or acceptors, the functional groups present on AC-Ws were examined first. If the hydrogen donor comes from the AC-Ws, the adsorption capacity could significantly shift at a pH of around 4, specifically if the carboxyl group loses its proton. Nevertheless, the adsorption capacity didn't alter much at this pH. Evidence that the additive donates hydrogen during adsorption is shown by the considerable reduction in adsorption ability as the pH comes closer to 9.6 (refer to Table 2). Additionally, since the chemical properties of the phenolic groups on the AC-Ws and the additive are alike, the hydrogen atom of the phenolic group on the AC-Ws has the possibility of donating hydrogen to the oxygen atom of the additive at pH 9.6. see Figure 13.

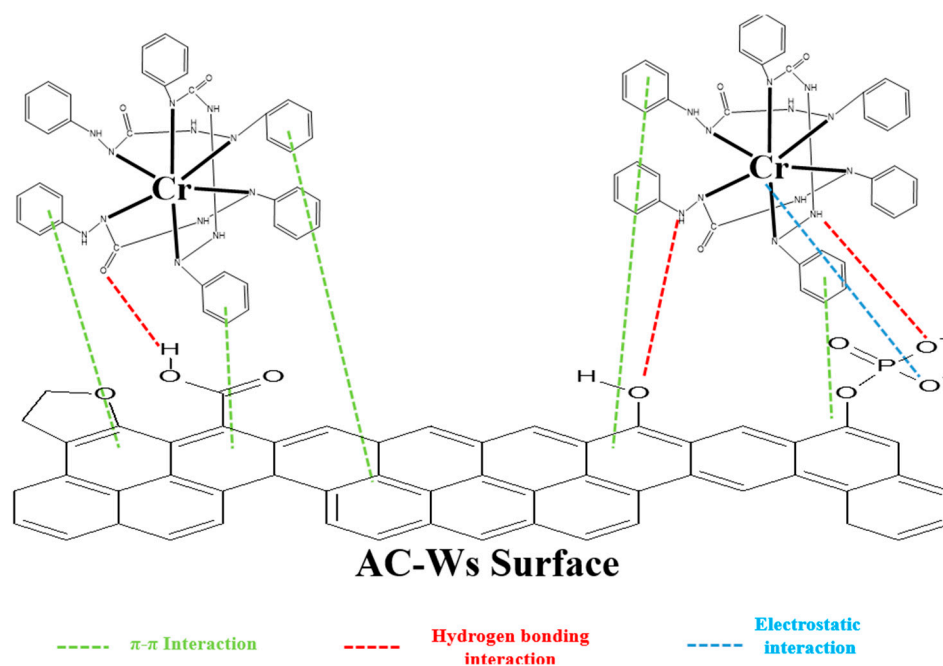


**Figure 13.** The adsorption process mechanism of Cr(VI) on AC-Ws.

### 3.10. Reusing Test of AC-Ws

Financial and ecological considerations associated with adsorbent materials have emphasized the significance of recycling bio-sorbents. As demonstrated in Figure 14, there is a decline in the adsorption capacity between the first and last cycles. Specifically, the adsorption capacity of AC-Ws decreased from 52.58 by 15.33 mg/g of Cr(VI) due to the reduction of its specific surface. Nevertheless, the remarkable adsorption and regeneration performance of AC-Ws highlights its potential for use in ecological applications, particularly in wastewater treatment.

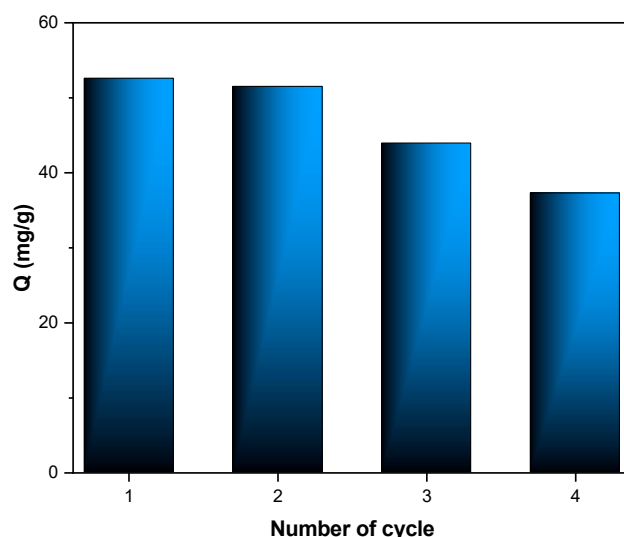


**Figure 14.** Regeneration cycles effect on the AC-Ws adsorption capacity. [AC-Ws] = 0.2 g/L; V = 50 mL, [Cr(VI)] = 2 mg/L and temperature: 298 K.

### 3.11. Mechanistic Study

Physical and chemical adsorption are the two main categories into which adsorption methods onto activated carbon can be generally divided. The basis for each category is the type of contact and the target pollutant's affinity for particular functional groups [62]. For instance, a chemical reaction or the bonding of the adsorbate and functional groups embedded on the surface of the adsorbent mediate chemical adsorption [63]. Quantum calculations were used to investigate the mechanism of adsorption processes of the chromium (VI) complex on the prepared activated carbon (AC) surface. As seen in Figure 15, the modified chitosan and alginate were combined to create this prepared model for the synthesized components.

The adsorption energy of both forms of chromium, Cr(VI) single atom and Cr(VI) complex, on the AC surface was calculated using Equation (1), and the optimized structures are illustrated in Figure 16. The adsorption energies are 0.51 and 24.72 kcal/mol for the Cr(VI) single atom and Cr(VI) complex, respectively. The adsorption energy values are a tool to explain the nature of the adsorption process. In the case of physisorption, the value of  $E_a$  is less than 1.673 kcal/mol, while in chemisorption higher than this limit [14,64,65]. These findings indicate that the adsorption of a Cr(VI) single atom will be through physisorption while the Cr(VI) complex will be adsorbed by strong interaction which is confirmed by the larger positive adsorption energy and can be explained by the possible hydrogen interaction between hydrogen atoms on the Cr(VI) complex and the oxygen atoms on the prepared AC surface [66]. The suggested mechanism for the adsorption of the Cr(VI) complex onto the prepared AC surface is carried out in three steps [63]. Diffusion of the Cr(VI) complex from the solution to the outside surface of the adsorbent is the initial phase. The penetration of the Cr(VI) complex into the inside of the adsorbent is the second process, which is slower than the first and is governed by the rate of diffusion. Finally, the final adsorption equilibrium phase constitutes the third stage.

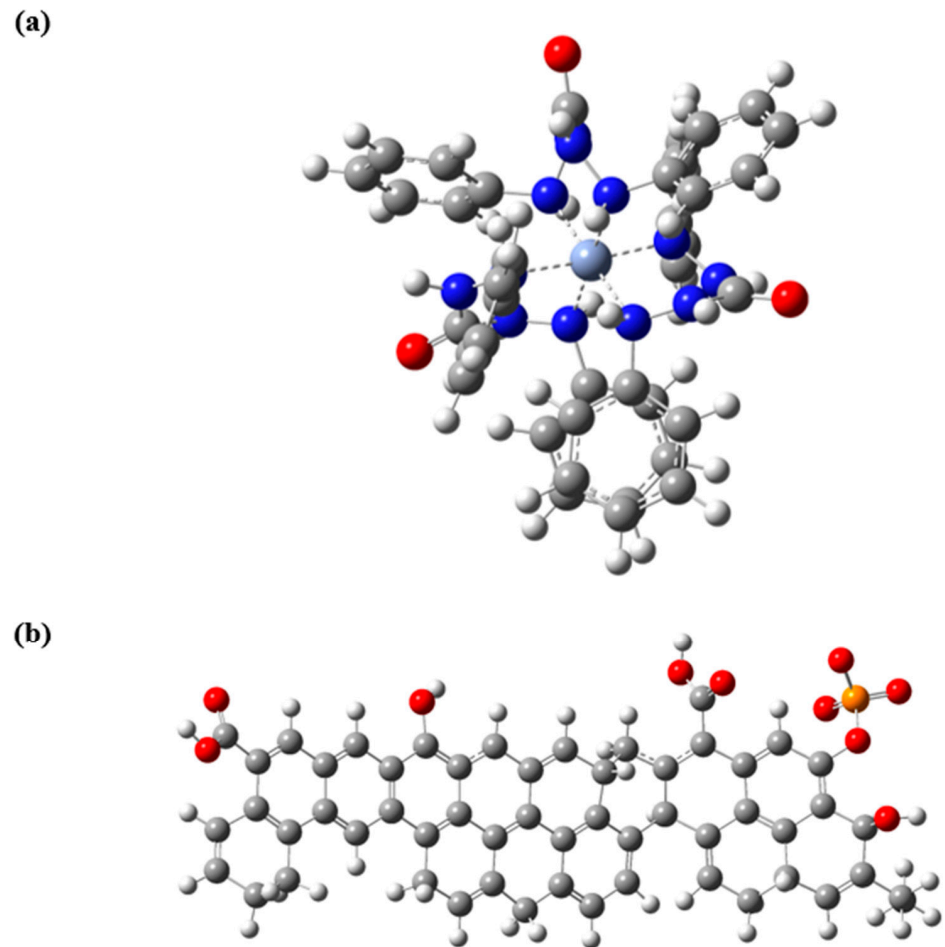


**Figure 15.** Molecular structure of (a) Cr(VI) complex and (b) prepared AC surface.

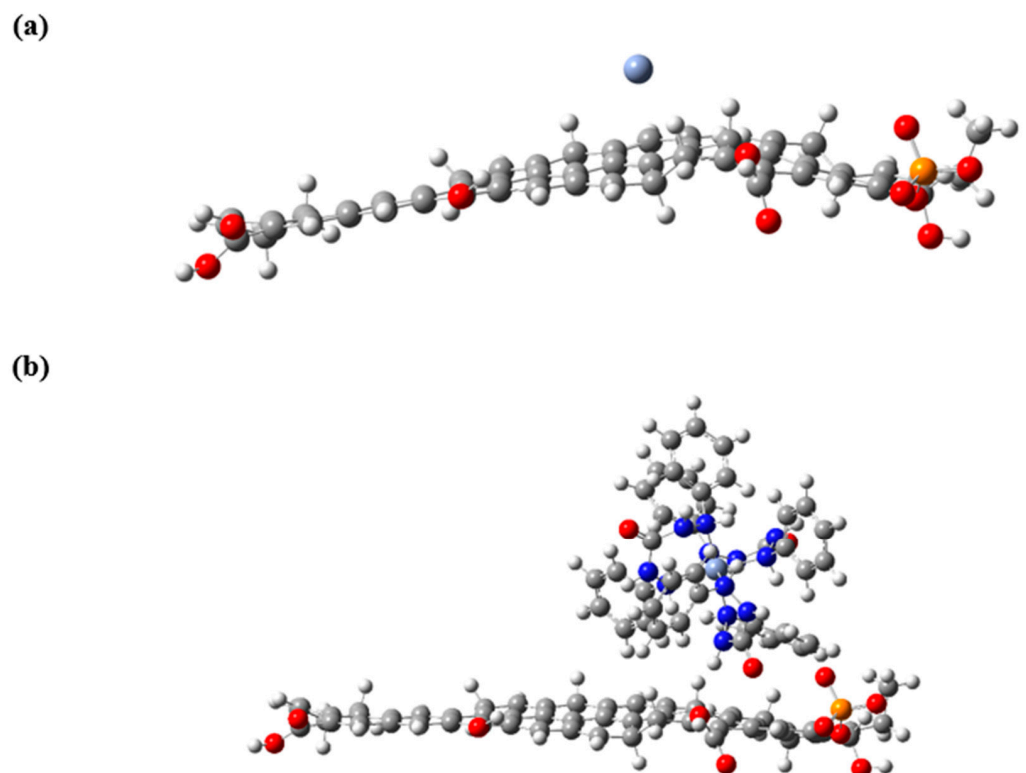


**Figure 16.** Adsorption process of (a) Cr(VI) atom and (b) Cr(VI) complex on prepared AC surface.

Non-covalent interactions (NCI) investigations were undertaken to reveal the nature of the interaction between the Cr(VI) single atom and Cr(VI) complex on the synthesized AC surface, and the findings are shown in Figure 17. In the case of the Cr(VI) single atom, a green surface was located between chromium and the AC-Ws surface confirming that the adsorption process will be performed through the vdW interactions. The presence of a blue surface between oxygen on the AC-Ws surface and hydrogen atoms on the Cr(VI) complex confirms the presence of a strong interaction through hydrogen bonds. The green surface between the Cr(VI) complex and the prepared AC surface indicates that the vdW interactions will be used for the adsorption process. Based on the previous discussion, it is possible to conclude that the picked-up results assist us in understanding the adsorption process of the presented material due to the fact they are in good agreement with the offered experimental data.

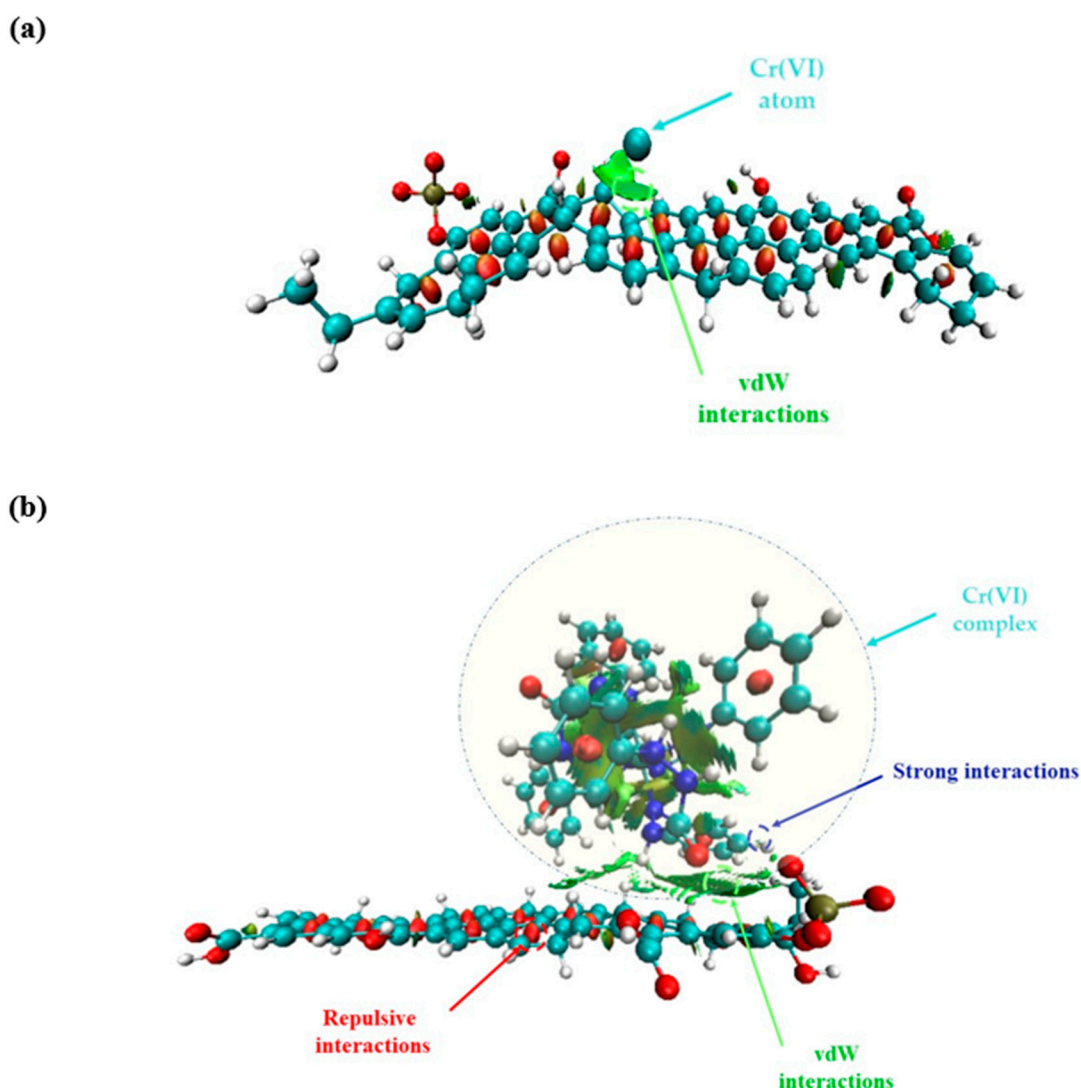


**Figure 17.** NCI isosurfaces of the adsorption of (a) Cr(VI) atom and (b) Cr(VI) complex into the AC-Ws surface. ( $s = 0.30$ ).

#### 4. Conclusions

The study aimed to create a low-cost and environmentally friendly adsorbent using walnut shell activated carbon (AC-Ws) prepared by the chemical activation method. Characterization results confirmed the successful synthesis of AC-Ws, which was then applied to remove Cr(VI) presented in aqueous solutions by optimizing the adsorption process using central composite design (CCD) and RSM methodology. The optimal conditions for

adsorption were found to be at pH 4, AC-Ws dosage of 0.23 g/L, a temperature of 25 °C, and a Cr(VI) concentration of 2 mg/L. The elimination efficiency and desirability function under these circumstances were 93% and 1.00, respectively. The adsorption process was described well by Langmuir and PSO models for isotherm and kinetics, respectively. Thermodynamic analysis showed that the adsorption process is spontaneous and exothermic. In conclusion, the synthesized AC-Ws is an efficient material for treating hazardous heavy metal wastewater before its release into the environment. Quantum simulations and NCI studies were carried out to shed further light on the Cr(VI) atom's adsorption mechanism and its complex shape on the produced AC-Ws surface. The results obtained are in good accord with reported experimental results.

**Author Contributions:** Conceptualization, H.Y. and M.E.h.; methodology, H.Y.; E.m.E.m. and T.B.; resources, S.R., M.E.H. and M.E.h.; software, M.E.H. writing—original draft preparation, H.Y., M.E.H. and L.B.; writing—review and editing, M.E.h. and L.B.; supervision, M.E.h. All authors have read and agreed to the published version of the manuscript.

**Funding:** This research received no external funding.

**Institutional Review Board Statement:** Not applicable.

**Informed Consent Statement:** Not applicable.

**Data Availability Statement:** The raw data supporting the conclusions of this article will be made available by the authors on request.

**Acknowledgments:** We are thankful to Cadi Ayyad University and the analysis & Characterization center at Cadi Ayyad University for providing the necessary facilities for research work.

**Conflicts of Interest:** The authors declare no conflict of interest.

## References

1. Zhang, L.; Fang, M. Nanomaterials in Pollution Trace Detection and Environmental Improvement. *Nano Today* **2010**, *5*, 128–142. [[CrossRef](#)]
2. Cho, D.-W.; Chon, C.-M.; Kim, Y.; Jeon, B.-H.; Schwartz, F.W.; Lee, E.-S.; Song, H. Adsorption of Nitrate and Cr(VI) by Cationic Polymer-Modified Granular Activated Carbon. *Chem. Eng. J.* **2011**, *175*, 298–305. [[CrossRef](#)]
3. Kleinberg, M.N.; Thamaraiselvan, C.; Powell, C.D.; Ronen, A.; Arnusch, C.J. Reduction of Cr(VI) to Cr(III) by Activated Carbon Cloth through Adsorption and Electrochemical Processes. *ACS Appl. Eng. Mater.* **2023**, *1*, 901–912. [[CrossRef](#)]
4. Yang, J.; Yu, K.; Liu, C. Chromium Immobilization in Soil Using Quaternary Ammonium Cations Modified Montmorillonite: Characterization and Mechanism. *J. Hazard. Mater.* **2017**, *321*, 73–80. [[CrossRef](#)] [[PubMed](#)]
5. Garg, U.K.; Kaur, M.P.; Garg, V.K.; Sud, D. Removal of Hexavalent Chromium from Aqueous Solution by Agricultural Waste Biomass. *J. Hazard. Mater.* **2007**, *140*, 60–68. [[CrossRef](#)] [[PubMed](#)]
6. Abedi, F.; Dubé, M.A.; Kruczek, B. Adsorption of Heavy Metals on the Surface of Nanofiltration Membranes: “A Curse or Blessing”? *J. Membr. Sci.* **2023**, *685*, 121988. [[CrossRef](#)]
7. Yang, J.; Yu, M.; Qiu, T. Adsorption Thermodynamics and Kinetics of Cr(VI) on KIP210 Resin. *J. Ind. Eng. Chem.* **2014**, *20*, 480–486. [[CrossRef](#)]
8. Zhao, D.; Yu, Y.; Chen, J.P. Zirconium/Polyvinyl Alcohol Modified Flat-Sheet Polyvinylidene Fluoride Membrane for Decontamination of Arsenic: Material Design and Optimization, Study of Mechanisms, and Application Prospects. *Chemosphere* **2016**, *155*, 630–639. [[CrossRef](#)]
9. Lv, Y.; Chang, K.; Wu, H.; Fang, P.; Chen, C.; Liao, Q. Highly Efficient Scavenging of Cr(VI) by Two-Dimensional Titanium Carbide Nanosheets: Kinetics, Isotherms and Thermodynamics Analysis. *Water Sci. Technol.* **2021**, *84*, 2446–2456. [[CrossRef](#)]
10. Wang, X.; Chen, M.; Nayanathara, R.M.O.; Zhang, Z.; Zhang, X. Tune Wastepaper to Hydrophobic Membranes through Metal-Ion-Induced Lignocellulose Nanofibril Crosslinking for Oil-Water Separation. *Carbohydr. Polym. Technol. Appl.* **2023**, *6*, 100377. [[CrossRef](#)]
11. Pazireh, S.; Dehqan, A.; Zinadini, S.; Zinatizadeh, A.A.; Vatanpour, V. Rosemary Particle as a New Green Additive to Improve Polysulfone Membrane Separation Performance in Removal of Organic Pollutants. *Sep. Purif. Technol.* **2024**, *334*, 126015. [[CrossRef](#)]
12. He, G.; Xiao, Y.; Du, H. An Overview and Recent Progress in Photocatalytic Cr(VI) Reduction and Hydrogen Evolution. *Int. J. Hydrogen Energy* **2024**, *53*, 633–646. [[CrossRef](#)]
13. Tzou, Y.M.; Wang, S.L.; Wang, M.K. Fluorescent Light Induced Cr(VI) Reduction by Citrate in the Presence of TiO<sub>2</sub> and Ferric Ions. *Colloids Surf. A Physicochem. Eng. Asp.* **2005**, *253*, 15–22. [[CrossRef](#)]

14. Basnet, P.; Ojha, P.K.; Gyawali, D.; Ghimire, K.N.; Paudyal, H. Thermochemical Study of Cr(VI) Sequestration onto Chemically Modified Areca Catechu and Its Recovery by Desorptive Precipitation Method. *Heliyon* **2022**, *8*, e10305. [[CrossRef](#)] [[PubMed](#)]
15. Cao, J.; Shi, Y.; Xin, J.; Kong, S.; Wang, X. Application of Microbial Fuel Cells with Tungsten-Based Semiconductor Modified Electrode in the Treatment of Cr (VI) Pollutions. *Biochem. Eng. J.* **2023**, *198*, 109034. [[CrossRef](#)]
16. Youssef, H.M.; Abdulhamed, Y.K.; Abu El-Reash, G.M.; Yousef, T.A. Cr(III) and Ni(II) Complexes of Isatin-Hydrazone Ligand: Preparation, Characterization, DFT Studies, Biological Activity, and Ion-Flotation Separation of Ni(II). *Inorg. Chem. Commun.* **2022**, *138*, 109278. [[CrossRef](#)]
17. Kubra, K.; Pavithra, V.; Gopal, B.; Janaswamy, S. An Integrated Chemical Approach for the Removal of Hazardous Cr(VI) and Other Contaminants of Tannery Wastewater: Biopolymer-Assisted Adsorption Separation and Conversion into Valuable Materials. *Sep. Purif. Technol.* **2024**, *330*, 125220. [[CrossRef](#)]
18. Su, K.; Hu, G.; Zhao, T.; Dong, H.; Yang, Y.; Pan, H.; Lin, Q. The Ultramicropore Biochar Derived from Waste Distiller's Grains for Wet-Process Phosphoric Acid Purification: Removal Performance and Mechanisms of Cr(VI). *Chemosphere* **2024**, *349*, 140877. [[CrossRef](#)] [[PubMed](#)]
19. Jahanban-Esfahlan, A.; Jahanban-Esfahlan, R.; Tabibiazar, M.; Roufegarinejad, L.; Amarowicz, R. Recent Advances in the Use of Walnut (*Juglans regia* L.) Shell as a Valuable Plant-Based Bio-Sorbent for the Removal of Hazardous Materials. *RSC Adv.* **2020**, *10*, 7026–7047. [[CrossRef](#)]
20. Ndoun, M.C.; Knopf, A.; Preisendanz, H.E.; Vozenilek, N.; Elliott, H.A.; Mashtare, M.L.; Velegol, S.; Veith, T.L.; Williams, C.F. Fixed Bed Column Experiments Using Cotton Gin Waste and Walnut Shells-Derived Biochar as Low-Cost Solutions to Removing Pharmaceuticals from Aqueous Solutions. *Chemosphere* **2023**, *330*, 138591. [[CrossRef](#)]
21. Banerjee, M.; Basu, R.K.; Das, S.K. Cr(VI) Adsorption by a Green Adsorbent Walnut Shell: Adsorption Studies, Regeneration Studies, Scale-up Design and Economic Feasibility. *Process Saf. Environ. Prot.* **2018**, *116*, 693–702. [[CrossRef](#)]
22. Soto-Maldonado, C.; Caballero-Valdés, E.; Santis-Bernal, J.; Jara-Quezada, J.; Fuentes-Viveros, L.; Zúñiga-Hansen, M.E. Potential of Solid Wastes from the Walnut Industry: Extraction Conditions to Evaluate the Antioxidant and Bioherbicidal Activities. *Electron. J. Biotechnol.* **2022**, *58*, 25–36. [[CrossRef](#)]
23. Jiang, Y. Preparation of Activated Carbon from Walnut Shell and Its Application in Industrial Wastewater. *AIP Conf. Proc.* **2017**, *1839*, 020063-1–020063-4. [[CrossRef](#)]
24. Gao, X.; Wu, L.; Wan, W.; Xu, Q.; Li, Z. Preparation of Activated Carbons from Walnut Shell by Fast Activation with H<sub>3</sub>PO<sub>4</sub>: Influence of Fluidization of Particles. *Int. J. Chem. React. Eng.* **2018**, *16*, 20170074. [[CrossRef](#)]
25. Sanati, A.M.; Kamari, S.; Ghorbani, F. Application of Response Surface Methodology for Optimization of Cadmium Adsorption from Aqueous Solutions by Fe<sub>3</sub>O<sub>4</sub>@SiO<sub>2</sub>@APTMS Core-Shell Magnetic Nanohybrid. *Surf. Interfaces* **2019**, *17*, 100374. [[CrossRef](#)]
26. El Mouchtari, E.M.; Daou, C.; Rafqah, S.; Najjar, F.; Anane, H.; Piram, A.; Hamade, A.; Briche, S.; Wong-Wah-Chung, P. TiO<sub>2</sub> and Activated Carbon of Argania Spinosa Tree Nutshells Composites for the Adsorption Photocatalysis Removal of Pharmaceuticals from Aqueous Solution. *J. Photochem. Photobiol. A Chem.* **2020**, *388*, 112183. [[CrossRef](#)]
27. Yazid, H.; Bouzid, T.; El Himri, M.; Regti, A.; El Haddad, M. Bisphenol A (BPA) Remediation Using Walnut Shell as Activated Carbon Employing Experimental Design for Parameter Optimization and Theoretical Study to Establish the Adsorption Mechanism. *Inorg. Chem. Commun.* **2024**, *161*, 112064. [[CrossRef](#)]
28. Regti, A.; Lakbaibi, Z.; Ben El Ayouchia, H.; El Haddad, M.; Laamari, M.R.; El Himri, M.; Haounati, R. Hybrid Methods Combining Computational and Experimental Measurements for the Uptake of Eriochrome Black T Dye Utilising Fish Scales. *Int. J. Environ. Anal. Chem.* **2023**, *103*, 4549–4568. [[CrossRef](#)]
29. Suryati, L.; Sulistyarti, H.; Atikah, A. Development of Spectrophotometric Method for Determination of Chromium Species Using Hypochlorite Agent Based on the Formation of Cr(VI)-Diphenylcarbazide Complex. *J. Pure App. Chem. Res.* **2015**, *4*, 34–41. [[CrossRef](#)]
30. Wildman, J.; Repiščák, P.; Paterson, M.J.; Galbraith, I. General Force-Field Parametrization Scheme for Molecular Dynamics Simulations of Conjugated Materials in Solution. *J. Chem. Theory Comput.* **2016**, *12*, 3813–3824. [[CrossRef](#)]
31. Perdew, J.P.; Burke, K.; Ernzerhof, M. Generalized Gradient Approximation Made Simple. *Phys. Rev. Lett.* **1996**, *77*, 3865–3868. [[CrossRef](#)] [[PubMed](#)]
32. Lu, T.; Chen, F. Multiwfn: A Multifunctional Wavefunction Analyzer. *J. Comput. Chem.* **2012**, *33*, 580–592. [[CrossRef](#)] [[PubMed](#)]
33. Humphrey, W.; Dalke, A.; Schulten, K. VMD: Visual Molecular Dynamics. *J. Mol. Graph.* **1996**, *14*, 33–38. [[CrossRef](#)] [[PubMed](#)]
34. Johnson, E.R.; Keinan, S.; Mori-Sánchez, P.; Contreras-García, J.; Cohen, A.J.; Yang, W. Revealing Noncovalent Interactions. *J. Am. Chem. Soc.* **2010**, *132*, 6498–6506. [[CrossRef](#)] [[PubMed](#)]
35. Nyberg, J.; Karlsson, M.O.; Hooker, A.C. Simultaneous Optimal Experimental Design on Dose and Sample Times. *J. Pharmacokinet. Pharmacodyn.* **2009**, *36*, 125–145. [[CrossRef](#)] [[PubMed](#)]
36. Ahmad Isiyaka, H.; Jumbri, K.; Soraya Sambudi, N.; Uba Zango, Z.; Ain Fathihah Binti Abdullah, N.; Saad, B. Effective Adsorption of Metolachlor Herbicide by MIL-53(Al) Metal-Organic Framework: Optimization, Validation and Molecular Docking Simulation Studies. *Environ. Nanotechnol. Monit. Manag.* **2022**, *18*, 100663. [[CrossRef](#)]
37. Goertzen, S.L.; Thériault, K.D.; Oickle, A.M.; Tarasuk, A.C.; Andreas, H.A. Standardization of the Boehm Titration. Part I. CO<sub>2</sub> Expulsion and Endpoint Determination. *Carbon* **2010**, *48*, 1252–1261. [[CrossRef](#)]

38. Koyuncu, F.; Güzel, F.; İnal, İ.İ.G. High Surface Area and Supermicroporous Activated Carbon from Capsicum (*Capsicum annuum* L.) Industrial Processing Pulp via Single-Step KOH-Catalyzed Pyrolysis: Production Optimization, Characterization and Its Some Water Pollutants Removal and Supercapacitor Performance. *Diam. Relat. Mater.* **2022**, *124*, 108920. [[CrossRef](#)]
39. Rose, P.K.; Poonia, V.; Kumar, R.; Kataria, N.; Sharma, P.; Lamba, J.; Bhattacharya, P. Congo Red Dye Removal Using Modified Banana Leaves: Adsorption Equilibrium, Kinetics, and Reusability Analysis. *Groundw. Sustain. Dev.* **2023**, *23*, 101005. [[CrossRef](#)]
40. Huang, T.; Song, D.; Yang, C.; Zhang, S. Nonthermal Plasma-Irradiated Polyvalent Ferromanganese Binary Hydro(Oxide) for the Removal of Uranyl Ions from Wastewater. *Environ. Res.* **2023**, *217*, 114911. [[CrossRef](#)]
41. Zafar, F.F.; Barati, B.; Rasoulzadeh, H.; Sheikhmohammadi, A.; Wang, S.; Chen, H. Adsorption Kinetics Analysis and Optimization of Bisphenol A onto Magnetic Activated Carbon with Shrimp Shell Based Precursor. *Biomass Bioenergy* **2022**, *166*, 106604. [[CrossRef](#)]
42. Zerhouni, J.; Rhazi Filali, F.; Naciri Bennani, M.; Qabaqous, O.; Bouymajane, A.; Houssaini, J.; Allaoui, S.; Benhallam, F. Study of the Effect of Acid-Base Character of the Lamellar Double Hydroxides “Zn<sub>3</sub>Al-CO<sub>3</sub>” and of the “Ghassoul” Clay on Their Redox Potential and Antimicrobial Activities. *Iran. J. Mater. Sci. Eng.* **2021**, *18*, 1–13. [[CrossRef](#)]
43. Chen, S.; Yue, Q.; Gao, B.; Li, Q.; Xu, X. Removal of Cr(VI) from Aqueous Solution Using Modified Corn Stalks: Characteristic, Equilibrium, Kinetic and Thermodynamic Study. *Chem. Eng. J.* **2011**, *168*, 909–917. [[CrossRef](#)]
44. Wu, Y.; Luo, H.; Wang, H.; Wang, C.; Zhang, J.; Zhang, Z. Adsorption of Hexavalent Chromium from Aqueous Solutions by Graphene Modified with Cetyltrimethylammonium Bromide. *J. Colloid Interface Sci.* **2013**, *394*, 183–191. [[CrossRef](#)] [[PubMed](#)]
45. Ltifi, I.; Ayari, F.; Hassen, C.; Ayadi, M.T. Study of the Adsorption of Bright Green by a Natural Clay and Modified. *J. Mater. Sci. Eng.* **2016**, *5*, 317–324. [[CrossRef](#)]
46. Grich, A.; Bouzid, T.; Naboulsi, A.; Regti, A.; Tahiri, A.A.; El Himri, M.; El Haddad, M. Preparation of Low-Cost Activated Carbon from Doum Fiber (*Chamaerops humilis*) for the Removal of Methylene Blue: Optimization Process by DOE/FFD Design, Characterization, and Mechanism. *J. Mol. Struct.* **2024**, *1295*, 136534. [[CrossRef](#)]
47. Khan, A.A.; Iqbal, J.; Bashir, M.T.; Amin, M.T.; Sikandar, M.A.; Rahman, M.M.; Arifuzzman, M. Synthesis, Characterization, and Performance of Nano-Metal-Oxide (Al<sub>2</sub>O<sub>3</sub>) Blended Biochar for the Removal of Iron from Contaminated Water for Enhanced Kinetic and Adsorption Studies. *Processes* **2023**, *11*, 3423. [[CrossRef](#)]
48. Karthikeyan, T.; Rajgopal, S.; Miranda, L. Chromium(VI) Adsorption from Aqueous Solution by Sawdust Activated Carbon. *J. Hazard. Mater.* **2005**, *124*, 192–199. [[CrossRef](#)]
49. Yang, J.; Yu, M.; Chen, W. Adsorption of Hexavalent Chromium from Aqueous Solution by Activated Carbon Prepared from Longan Seed: Kinetics, Equilibrium and Thermodynamics. *J. Ind. Eng. Chem.* **2015**, *21*, 414–422. [[CrossRef](#)]
50. Noufel, K.; Djebri, N.; Boukhalifa, N.; Boutahala, M.; Dakhouche, A. Removal of Bisphenol A and Trichlorophenol from Aqueous Solutions by Adsorption with Organically Modified Bentonite, Activated Carbon Composites: A Comparative Study in Single and Binary Systems. *Groundw. Sustain. Dev.* **2020**, *11*, 100477. [[CrossRef](#)]
51. Yazid, H.; Achour, Y.; El Kassimi, A.; Nadir, I.; El Himri, M.; Laamari, M.; El Haddad, M. Removal of Congo Red from Aqueous Solution Using Cuttlefish Bone Powder. *PCR* **2021**, *9*, 565–577. [[CrossRef](#)]
52. Mejbar, F.; Miyah, Y.; Benjelloun, M.; Ssouni, S.; Saka, K.; Lahrichi, A.; Zerrouq, F. High-Performance of Cu@eggshells for Toxic Dyes Catalytic Wet Peroxide Oxidation: Kinetics, Design of Experiments, Regeneration, and Cost Analysis. *Case Stud. Chem. Environ. Eng.* **2024**, *9*, 100572. [[CrossRef](#)]
53. Wang, C.; Xie, J.; Zheng, M.; Zhu, J.; Shi, C. Preparation of Mesoporous Biochar from Cornstalk for the Chromium (VI) Elimination by Using One-Step Hydrothermal Carbonation. *J. Anal. Methods Chem.* **2021**, *2021*, 3418887. [[CrossRef](#)]
54. Chandra Joshi, N.; Singh, A. Adsorptive Performances and Characterisations of Biologically Synthesised Zinc Oxide Based Nanosorbent (ZOBn). *Groundw. Sustain. Dev.* **2020**, *10*, 100325. [[CrossRef](#)]
55. Atieh, M.A. Removal of Chromium (VI) from Polluted Water Using Carbon Nanotubes Supported with Activated Carbon. *Procedia Environ. Sci.* **2011**, *4*, 281–293. [[CrossRef](#)]
56. Tang, Q.; Wu, H.; Zhou, M.; Yang, D. Preparation of a Novel High-Performance Lignin-Based Anionic Adsorption Resin for Efficient Removal of Cr(VI) in Aqueous Solutions. *Ind. Crop. Prod.* **2023**, *199*, 116720. [[CrossRef](#)]
57. Owlad, M.; Aroua, M.K.; Wan Daud, W.M.A. Hexavalent Chromium Adsorption on Impregnated Palm Shell Activated Carbon with Polyethyleneimine. *Bioresour. Technol.* **2010**, *101*, 5098–5103. [[CrossRef](#)] [[PubMed](#)]
58. Liang, S.; Jiao, W.; Zhang, D.; Zhang, H.; Qiao, R.; Liu, H.; Wang, M.; Chen, Y.; Zou, M.; Huang, Y.; et al. Phosphoramidic Acid Functionalized Silica Microspheres for Simultaneous Removal of Cr(VI), As(V) and Se(VI) from Aqueous Solutions Based on Molecular Geometry Match. *J. Environ. Chem. Eng.* **2023**, *11*, 110300. [[CrossRef](#)]
59. Giri, R.; Kumari, N.; Behera, M.; Sharma, A.; Kumar, S.; Kumar, N.; Singh, R. Adsorption of Hexavalent Chromium from Aqueous Solution Using Pomegranate Peel as Low-Cost Biosorbent. *Environ. Sustain.* **2021**, *4*, 401–417. [[CrossRef](#)]
60. Jayasuriya, D.M.N.H.; Nadarajah, K. Understanding Association between Methylene Blue Dye and Biosorbent: Palmyrah Sprout Casing in Adsorption Process in Aqueous Phase. *Water Sci. Eng.* **2023**, *16*, 154–164. [[CrossRef](#)]
61. Balakrishnan, A.; Jacob, M.M.; Dayanandan, N.; Chinthala, M.; Ponnuchamy, M.; Vo, D.-V.N.; Appunni, S.; Gajendhran, A.S. Chitosan/Metal Organic Frameworks for Environmental, Energy, and Bio-Medical Applications: A Review. *Mater. Adv.* **2023**, *4*, 5920–5947. [[CrossRef](#)]

62. Sellaoui, L.; Gómez-Avilés, A.; Dhaouadi, F.; Bedia, J.; Bonilla-Petriciolet, A.; Rtimi, S.; Belver, C. Adsorption of Emerging Pollutants on Lignin-Based Activated Carbon: Analysis of Adsorption Mechanism via Characterization, Kinetics and Equilibrium Studies. *Chem. Eng. J.* **2023**, *452*, 139399. [[CrossRef](#)]
63. Zhu, K.; Ma, J.; Cong, J.; Zhang, T.; Lei, H.; Xu, H.; Luo, Z.; Li, M. The Road to Reuse of Walnut By-Products: A Comprehensive Review of Bioactive Compounds, Extraction and Identification Methods, Biomedical and Industrial Applications. *Trends Food Sci. Technol.* **2024**, *143*, 104264. [[CrossRef](#)]
64. Ebisike, K.; Elvis Okoronkwo, A.; Kanayo Alaneme, K.; Jeremiah Akinribide, O. Thermodynamic Study of the Adsorption of Cd<sup>2+</sup> and Ni<sup>2+</sup> onto Chitosan—Silica Hybrid Aerogel from Aqueous Solution. *Results Chem.* **2023**, *5*, 100730. [[CrossRef](#)]
65. Inglezakis, V.J.; Zorpas, A.A. Heat of Adsorption, Adsorption Energy and Activation Energy in Adsorption and Ion Exchange Systems. *Desalin. Water Treat.* **2012**, *39*, 149–157. [[CrossRef](#)]
66. Garg, R.; Garg, R.; Sillanpää, M.; Alimuddin; Khan, M.A.; Mubarak, N.M.; Tan, Y.H. Rapid Adsorptive Removal of Chromium from Wastewater Using Walnut-Derived Biosorbents. *Sci. Rep.* **2023**, *13*, 6859. [[CrossRef](#)]

**Disclaimer/Publisher’s Note:** The statements, opinions and data contained in all publications are solely those of the individual author(s) and contributor(s) and not of MDPI and/or the editor(s). MDPI and/or the editor(s) disclaim responsibility for any injury to people or property resulting from any ideas, methods, instructions or products referred to in the content.